Math. Model. Nat. Phenom.
Vol. 7, No. 2, 2012, pp. 113–130
DOI: 10.1051/mmnp/20127210

On Numerical Solution of the Gardner–Ostrovsky Equation

M. A. Obregon[1], Y. A. Stepanyants[2*]

[1]E.T.S. Ingeniería Industrial, University of Malaga, Dr Ortiz Ramos s/n, 29071, Malaga, Spain

[2]Department of Mathematics and Computing, Faculty of Sciences, University of Southern Queensland Toowoomba, Australia

Abstract. A simple explicit numerical scheme is proposed for the solution of the Gardner–Ostrovsky equation $\left(u_t + cu_x + \alpha u u_x + \alpha_1 u^2 u_x + \beta u_{xxx}\right)_x = \gamma u$ which is also known as the extended rotation-modified Korteweg–de Vries (KdV) equation. This equation is used for the description of internal oceanic waves affected by Earth' rotation. Particular versions of this equation with zero some of coefficients, α, α_1, β, or γ are also known in numerous applications. The proposed numerical scheme is a further development of the well-known finite-difference scheme earlier used for the solution of the KdV equation. The scheme is of the second order accuracy both on temporal and spatial variables. The stability analysis of the scheme is presented for infinitesimal perturbations. The conditions for the calculations with the appropriate accuracy have been found. Examples of calculations with the periodic boundary conditions are presented to illustrate the robustness of the proposed scheme.

Keywords and phrases: KdV equation, Ostrovsky equation, soliton, terminal decay, Petviashvili method, numerical scheme

Mathematics Subject Classification: 35Q51, 35Q53, 35Q90, 37K40, 65Y20, 65Z05

1. Introduction

The model equation, dubbed here the Gardner–Ostrovsky (GO) equation (it is also known as the extended rotation-modified Korteweg–de Vries (KdV) equation), has been derived for the description of long internal waves of large amplitude [11]:

$$\frac{\partial}{\partial x}\left(\frac{\partial u}{\partial t} + c\frac{\partial u}{\partial x} + \alpha u\frac{\partial u}{\partial x} + \alpha_1 u^2\frac{\partial u}{\partial x} + \beta\frac{\partial^3 u}{\partial x^3}\right) = \gamma u, \tag{1.1}$$

where c is the velocity of dispersionless linear waves, α and α_1 are the coefficients of quadratic and cubic nonlinearities, respectively, and β and γ are the coefficients of small-scale and large-scale dispersion, respectively. The variable $u(x,t)$ describes a perturbation of the isopycnal surface – the surface of equal density – from its rest position.

This equation combines the dispersion effects due to nonhydrostaticity caused by the finiteness of the basin depth (the small-scale Boussinesq dispersion, proportional to β) and due to Earth's rotation

*Corresponding author. E-mail: Yury.Stepanyants@usq.edu.au

(the large-scale Coriolis dispersion, proportional to γ). The equation contains also two nonlinear terms proportional to α and α_1. The former one is the traditional quadratic nonlinear term appearing due to hydrodynamic nonlinearity, as in the KdV equation [22], whereas the latter term appears either when the first term becomes anomalously small (such situation may arise when the pycnocline is located near the half depth of the basin [2,11]), or when the GO equation is used as the model equation for the description of effects of strong nonlinearity caused by large-amplitude waves [16].

Equation (1.1) in the particular cases reduces to different well-known model equations: when $\gamma = 0$, this equation represents the Gardner equation, which reduces, in turn, to the KdV equation when $\alpha_1 = 0$. If $\gamma \neq 0$, but $\alpha_1 = 0$, Eq. (1.1) represents the Ostrovsky equation which is widely used currently in application to many physical problems, including the description of surface and internal waves in rotating oceans [14] (see, also [9,15]), magneto-sonic waves in rotating plasma [13], waves in relaxing media [21], etc. When $\gamma = 0$, both the KdV and Gardner equations are completely integrable (see, e.g., [1]), whereas with $\gamma \neq 0$ the equations become non-integrable. In such situation the problem of numerical solution of Eq. (1.1) becomes very topical. The most advanced study on the construction of effective numerical scheme for the solution of KdV equation has been published in the book by Berezin [3]. Several different numerical codes were analysed in that book and stability criteria for them have been derived. Various numerical codes were also developed for the solution of the Ostrovsky [4,6–8,10,23] and GO equations [11]. Nevertheless, the effectiveness of the published codes has not been thoroughly investigated and the results obtained were not compared either with each other or against approximate analytical solutions. Here we propose a new numerical code for the solution of the GO equation. The code is based on the explicit numerical scheme of the second order of accuracy in the temporal and spatial variables. The stability of the numerical scheme is also studied and the condition providing reliable calculations is derived. Results of computations within the framework of the proposed scheme are compared against stationary solutions and approximate analytical solutions for the terminal decay of solitary pulses.

2. Numerical scheme for the solution of the Gardner–Ostrovsky equation

First of all, for the sake of simplicity, but without loss of generality, we remove the linear term proportional to c from Eq. (1.1). This can be done by means of the Galilean transformation of variables $x_n = x_0 - c\,t_0$ and $t_n = t_0$. We omit further index n and present Eq. (1.1) in the form

$$\frac{\partial u}{\partial t} + \alpha u \frac{\partial u}{\partial x} + \alpha_1 u^2 \frac{\partial u}{\partial x} + \beta \frac{\partial^3 u}{\partial x^3} = \gamma \left[\int_0^x u(x',t)\,dx' - \langle v \rangle \right], \tag{2.1}$$

where $v(x,t) = \int_0^x u(x',t)\,dx'$ is the primitive of the function $u(x,t)$ and $\langle v \rangle \equiv \frac{1}{L}\int_0^L v(x,t)\,dx$ is the mean value of the function $v(x,t)$ on the interval $0 \le x \le L$. Such form of Eq. (1.1) is dictated by the property of the GO equation which states that for smooth periodic perturbations the mean value of u in the indicated interval is zero: $\langle u \rangle \equiv \frac{1}{L}\int_0^L u(x,t)\,dx = 0$ (see, for instance, [9, 15, 19] where this property is explained for the Ostrovsky equation which is a particular case of the GO equation (1.1) with $\alpha_1 = 0$).

To approximate partial derivatives in Eq. (2.1) we apply the following central differences:

$$\frac{\partial u}{\partial t} \to \frac{u^{n+1} - u^{n-1}}{2\tau}, \quad \frac{\partial u}{\partial x} \to \frac{u_{j+1} - u_{j-1}}{2h}, \quad \frac{\partial^3 u}{\partial x^3} \to \frac{u_{j+2} - 2(u_{j+1} - u_{j-1}) - u_{j-2}}{2h^3}, \tag{2.2}$$

where τ and $h = L/N_x$ are temporal and spatial steps of integration, so that $t_n = n\tau$, and $x_j = jh$; N_x is the total number of nodes on the period L. The integer number n characterises the time layer and varies from 0 to some number N_t, which corresponds to the desired instant of time $t = \tau N_t$. Another integer number j designates the spatial node of function $u(x,t)$ and varies from 1 to N_x. The replacement of the

partial derivatives by the differences as per Eq. (2.2) guarantees that the derivatives are approximated with the accuracy up to τ^2 and h^2. Indeed, the Taylor series of $u_{j\pm1}$ around the point $x_j = hj$ is:

$$u_{j\pm1} = u_j \pm \frac{\partial u}{\partial x}\Big|_{x_j} \cdot h + \frac{\partial^2 u}{\partial x^2}\Big|_{x_j} \cdot \frac{h^2}{2!} \pm \frac{\partial^3 u}{\partial x^3}\Big|_{x_j} \cdot \frac{h^3}{3!} + \frac{\partial^4 u}{\partial x^4}\Big|_{x_j} \cdot \frac{h^4}{4!} + \dots$$

Hence,

$$\frac{\partial u}{\partial x} \to \frac{u_{j+1} - u_{j-1}}{2h} = \frac{\partial u}{\partial x} + \frac{\partial^3 u}{\partial x^3}\frac{h^2}{6} + o(h^2).$$

So, if $h \ll 1$, then we have $\dfrac{u_{j+1} - u_{j-1}}{2h} \approx \dfrac{\partial u}{\partial x}$ up to h^2. Similarly for the time and third spatial derivatives we have, correspondingly:

$$\frac{u^{n+1} - u^{n-1}}{2\tau} = \frac{\partial u}{\partial t} + O(\tau^2), \qquad \frac{u_{j+2} - 2(u_{j+1} - u_{j-1}) - u_{j-2}}{2h^3} = \frac{\partial^3 u}{\partial x^3} + O(h^2).$$

The integrals in the right-hand side of Eq. (2.1) can be calculated by means of the trapezoidal rule:

$$\int_0^x u(x', t)\, dx \approx \frac{h}{2} \sum_{m=1}^{j} \left[u(x_m, t_n) + u(x_{m+1}, t_n) \right]. \tag{2.3}$$

Thus, the PDE (2.1) can be approximated by the following finite-difference equation:

$$\frac{u_j^{n+1} - u_j^{n-1}}{2\tau} + \left[\alpha u_j^n + \alpha_1 \left(u_j^n\right)^2 \right] \frac{u_{j+1}^n - u_{j-1}^n}{2h} + \beta \frac{u_{j+2}^n - 2(u_{j+1}^n - u_{j-1}^n) - u_{j-2}^n}{2h^3} =$$

$$\gamma \left(v_j^n - \langle v \rangle \right), \tag{2.4}$$

where $v_j^n \approx \dfrac{h}{2} \displaystyle\sum_{m=1}^{j} \left(u_m^n + u_{m+1}^n \right)$ and $\langle v \rangle \approx \dfrac{1}{2N_x} \displaystyle\sum_{1=1}^{N_x} \left(v_l^n + v_{l+1}^n \right)$.

From Eq. (2.4) we find

$$u_j^{n+1} = u_j^{n-1} - \frac{\tau}{h} \left[\alpha u_j^n + \alpha_1 \left(u_j^n\right)^2 - \frac{2\beta}{h^2} \right] \left(u_{j+1}^n - u_{j-1}^n \right) - \frac{\beta\tau}{h^3} \left(u_{j+2}^n - u_{j-2}^n \right) +$$

$$\gamma\tau h \left[\sum_{m=1}^{j} \left(u_m^n + u_{m+1}^n \right) - \frac{1}{L} \sum_{1=1}^{N_x} \left(v_l^n + v_{l+1}^n \right) \right]. \tag{2.5}$$

The template for the calculations on the basis of the scheme (2.5) is presented in Fig. 1.

For the periodic boundary condition, $u(t, L) = u(t, 0)$, we put

$$u_0^n = u_{N_x}^n, \quad u_{-1}^n = u_{N_x-1}^n, \quad u_{N_x+1}^n = u_1^n, \quad u_{N_x+2}^n = u_2^n. \tag{2.6}$$

As one can, the routine application of the numerical scheme (2.5) presumes that the function $u(x_j, t_n)$ is known on two previous time layers n and $n-1$. However, the GO equation, in either form (1.1) or (2.1), is usually considered with the given initial condition, $u(0, x) = U(x)$, i.e. we have a function $U(x_j)$ on the time layer $n = 0$ only. To initiate the routine calculations on the basis of the two-layer template shown in Fig. 1, we need to prepare the function values at the next time layer for $n = 1$. This can be realised with the simplified numerical scheme of the first-order accuracy in time, but the second-order accuracy in x.

For the simplified numerical scheme we approximate time derivative by the backward difference instead of the central difference used above:

$$\frac{\partial u}{\partial t} \to \frac{u^n - u^{n-1}}{\tau}. \tag{2.7}$$

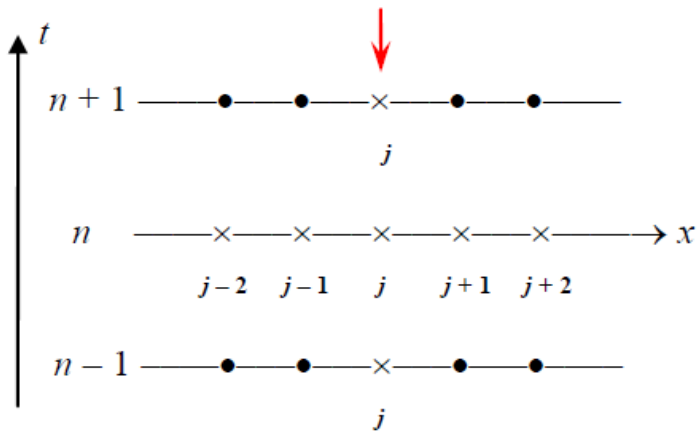

FIGURE 1. The template for the numerical scheme (2.5). Downward directed arrow above the node j indicates the node on the time layer $n+1$ where the function value is calculated using function values on two previous time layers n and $n-1$ in the nodes marked by crosses (the function values $u(x_j, t_n)$ in all nodes j are used on the time layer n to calculate the function $v(x_j, t_n)$).

All spatial derivatives remain the same as in Eqs. (2.1). With the help of the Taylor series for u^{n-1} it easy to see that

$$\frac{u^n - u^{n-1}}{\tau} = \frac{\partial u}{\partial t}(x_j, t_n) + O(\tau).$$

Thus, the PDE (2.1) can be approximated now by the following finite-difference equation:

$$\frac{u_j^n - u_j^{n-1}}{\tau} + \left[\alpha u_j^{n-1} + \alpha_1 \left(u_j^{n-1}\right)^2\right] \frac{u_{j+1}^{n-1} - u_{j-1}^{n-1}}{2h} + \beta \frac{u_{j+2}^{n-1} - 2(u_{j+1}^{n-1} - u_{j-1}^{n-1}) - u_{j-2}^{n-1}}{2h^3} =$$

$$\gamma \left(v_j^{n-1} - \langle v \rangle\right). \tag{2.8}$$

From this equation one can deduce

$$u_j^n = u_j^{n-1} - \frac{\tau}{2h}\left[\alpha u_j^{n-1} + \alpha_1 \left(u_j^{n-1}\right)^2 - \frac{2\beta}{h^2}\right]\left(u_{j+1}^{n-1} - u_{j-1}^{n-1}\right) - \frac{\beta\tau}{2h^3}\left(u_{j+2}^{n-1} - u_{j-2}^{n-1}\right) +$$

$$\frac{\gamma\tau h}{2}\left[\sum_{m=1}^{j}\left(u_m^{n-1} + u_{m+1}^{n-1}\right) - \frac{1}{L}\sum_{1=1}^{N_x}\left(v_l^{n-1} + v_{l+1}^{n-1}\right)\right]. \tag{2.9}$$

The template for this simplified scheme is shown in Fig. 2.

To achieve the appropriate accuracy in the calculation of the function $u(x_j, \tau)$ on the first time layer, one can perform several consecutive calculations with the smaller steps $\tau_2 = \tau/2, \tau_4 = \tau/4, \ldots$. After two successive calculations of the function $u(x_j, \tau)$ with different time steps, the discrepancy can be calculated (the number of required steps N_s to reach the time layer τ is inverse proportional to the value of the used small step $\tau_{N_s} = \tau/N_s$):

$$E = \sqrt{\sum_{j=1}^{N_x}\left[u_1(\tau, x_j) - u_2(\tau, x_j)\right]^2},$$

where $u_1(\tau, x_j)$ and $u_2(\tau, x_j)$ pertain to function calculations with two different time steps. If the discrepancy becomes less than the required value ε, then one may consider that the function $u(x_j, \tau)$ has been found on the first time layer $n = 1$ and the routine calculations can be initiated on the basis of the two-layer scheme (2.5). Examples of such calculations will be presented below.

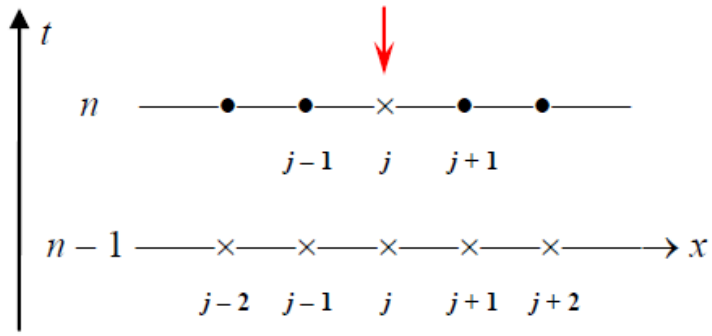

FIGURE 2. The template for the simplified numerical scheme (2.9).

3. Stability of the numerical scheme for the Gardner–Ostrovsky equation

Every time when a new numerical scheme is proposed, its stability should be investigated. In accordance with the well-known theorem, the convergence of a numerical solution to the solution of corresponding PDE follows from the correct numerical approximation of this PDE and stability of the used numerical code. If the stability is not investigated, then there is no guarantee that the obtained numerical solution has any relation to the solution of studied PDE.

Unfortunately, there are no general methods to investigate the stability of numerical schemes of nonlinear equations. In such situation, one can investigate the stability of a numerical scheme for the linearised equation, at least. Then, solutions of a nonlinear equation can be compared against the reference analytical solutions, if such are known. If not, one can only relay on its own intuition or reasonable character of the obtained numerical solution.

In this section we investigate the stability of the proposed numerical scheme for the linearised version of Eq. (2.1) with $\alpha = \alpha_1 = 0$. Let us look for a solution to the discrete version of this equation, Eq. (2.5), in the form $u_j^n = \lambda^n e^{ikj}$, where λ is an unknown number, k is the parameter (the number of a spatial harmonic), which varies from zero to π, and i is the imaginary unit. By substitution of this solution into Eq. (2.5) with $\alpha = \alpha_1 = 0$ we obtain after cancellation by $\lambda^n e^{ikj}$:

$$\lambda - \lambda^{-1} + \frac{\beta\tau}{h^3}\left(e^{2ik} - e^{-2ik}\right) - 2\frac{\beta\tau}{h^3}\left(e^{ik} - e^{-ik}\right) + \gamma\tau h e^{ik}\frac{1 + e^{ik}}{1 - e^{ik}} = 0. \tag{3.1}$$

This equation can be further reduced to the following quadratic equation for λ:

$$\lambda^2 - 4i\frac{\beta\tau}{h^3}\sin k(1 - \cos k)\left[1 + \frac{\gamma h^4}{4\beta}\frac{\cos 2k + i\sin 2k}{(1 - \cos k)^2}\right]\lambda - 1 = 0. \tag{3.2}$$

Solution to this equation is

$$\lambda_{1,2} = 2i\frac{\beta\tau}{h^3}\sin k(1 - \cos k)\left[1 + \frac{\gamma h^4}{4\beta}\frac{\cos 2k + i\sin 2k}{(1 - \cos k)^2}\right] \pm$$

$$\sqrt{1-4\left(\frac{\beta\tau}{h^3}\right)^2\sin^2 k(1-\cos k)^2\left[1+\frac{\gamma h^4}{4\beta}\frac{\cos 2k+i\sin 2k}{(1-\cos k)^2}\right]^2}. \tag{3.3}$$

The stability takes place when $|\lambda_{1,2}| \le 1$ (see, e.g., [3]). In the case of linearised Gardner or KdV equation, (i.e., when $\gamma = 0$), this condition can be fulfilled if we assume that the expression under the square root in non-negative, $1-4\left(\beta\tau/h^3\right)^2\sin^2 k(1-\cos k)^2 \ge 0$. Then, it is easy to see that $|\lambda_{1,2}| = 1$,and from this condition we find

$$\frac{\beta\tau}{h^3} \le \frac{1}{2|\sin k|(1-\cos k)|}.$$

The right-hand side of this inequality depends on the harmonic number k, but cannot be less than $2\sqrt{3}/9 \approx 0.385$. The minimum occurs at the most "dangerous" harmonic $k_d = 2\pi/3$. Thus, we arrive to the earlier derived criterion [3]: when $\tau < 0.385h^3/\beta$, the numerical scheme (2.5) with $\gamma = 0$ is stable with respect to small perturbations.

The situation with the analysis of the roots (3.3) becomes much more complicated when $\gamma \ne 0$. Any vivid form for the roots $|\lambda_{1,2}|$ convenient for the analysis was not found. However the dependence of $|\lambda_{1,2}|$ on the parameters k, $B \equiv \beta\tau/h^3$ and $\Gamma \equiv \gamma h^4/4\beta$ can be analysed numerically and graphically. Typical dependences of $|\lambda_{1,2}|$ on k for $B = 10^{-3}$ and $\Gamma = 10^{-3}$ are shown in Fig. 3. These two functions are mirror symmetric to each other with respect to the horizontal axis $|\lambda| = 1$. Independently of B and Γ they intersect at the points $k = \pi/2$ and π where both of them turn to unity. The roots $|\lambda_{1,2}|$ can be also presented as the 3D functions of k and B for different values of Γ. Figure 4 illustrates these functions for $\Gamma = 10^{-3}$ and B varying in the range $0 \le B \le 10^{-3}$.

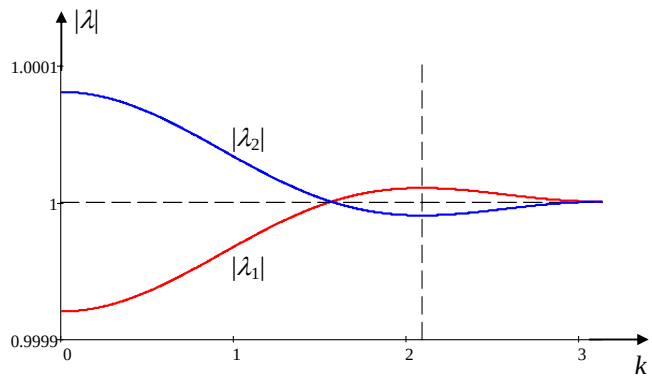

FIGURE 3. Dependences of $|\lambda_{1,2}|$ on k for $B = 10^{-3}$ and $\Gamma = 10^{-3}$ as per Eq. (3.3). The vertical dashed line shows the most "dangerous" wave number $k = 3\pi/2$ for $|\lambda_1|$, whereas the most "dangerous" wave number for $|\lambda_2|$ takes place at $k = 0$.

The analysis shows that the maxima of the functions $|\lambda_{1,2}|$ for all $\Gamma \ne 0$ are always greater than 1, which stands for that the numerical scheme (2.5) is unstable in principle. However, the growth rate of instability development can be reduced to extremely small value with the appropriate choice of the parameters B and Γ. In the result of that, the instability may not affect the calculations on such time intervals which are much less than the characteristic time of instability manifestation. As one can see from the plots shown above, the most dangerous instability may occur for $|\lambda_2|$ when $k \to 0$. If one puts $B = 10^{-3}$ and $\Gamma = 10^{-3}$ as in Fig. 3, then $|\lambda_2|_{max}$ exceeds 1 by less than 10^{-4}. This means that the error in computation of function $u(x,t)$ may reach 100% only after $\sim 10^4$ time steps. Hence, in the time

interval $t < 10^3\tau$ one can expect that in the worse case the error of numerical calculation will not exceed 10%, which may be quite appropriate accuracy in many cases.

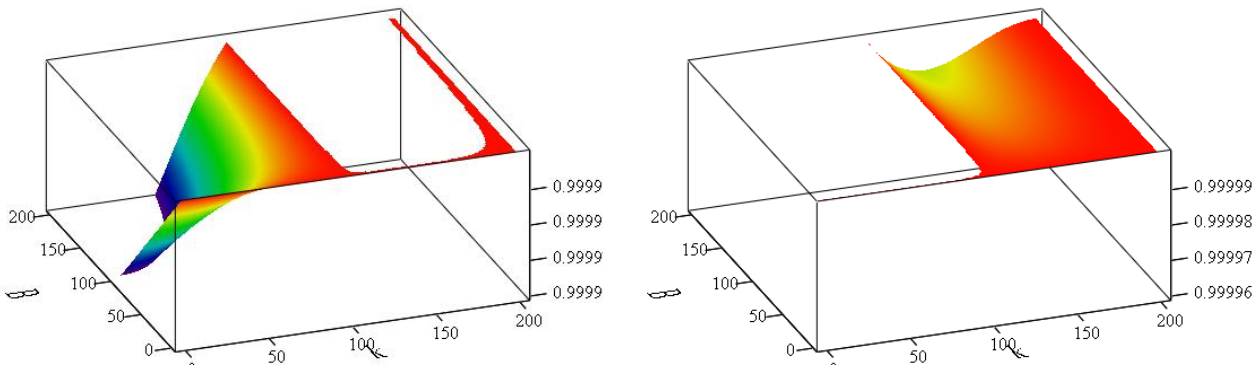

FIGURE 4. 3D plots of $|\lambda_{1,2}|$ on k and B for $\Gamma = 10^{-3}$ as per Eq. (3.3). The blank white regions on the top of each boxes show the function cuts at $|\lambda_{1,2}| = 1$.

4. Examples of numerical computations within the framework of the GO equation

To validate the robustness of the developed numerical code we have undertaken several runs with theoretically predictable results. We will check not only the behavior of a numerical solution in time and space, but test also the accuracy of computations with the help of conservation laws known for the GO equation.

As has been mentioned above [see text after Eq. (2.1)], all smooth solutions of the GO equation must satisfy to the zero mean value constraint:

$$I_1 \equiv \langle u \rangle = \frac{1}{L}\int_0^L u(x,t)\,dx = 0.$$

There are also some more integral quantities which are determined solely by the initial condition and are preserved in time. Among them the quantities of primary physical interests are the "energy" I_2 and Hamiltonian I_3 (cf. [9, 23]):

$$I_2 = \frac{1}{2}\int_0^L u^2(x,t)\,dx = 0, \qquad I_3 = \int_0^L \left(\frac{\alpha}{6}u^3 + \frac{\alpha_1}{12}u^2 - \frac{\beta}{2}u_x^2 + \frac{v^2}{2\gamma}\right) dx = 0,$$

where $v_x = \gamma u$.

Below we present a comparison of numerical data against theoretical predictions for some particular examples and show the accuracy of conservation for the integral quantities I_1, I_2, and I_3. We examine both cases of positive and negative small-scale dispersion, because the GO equation has different properties for these two cases. To avoid any confusion, we remind that the positive/negative dispersion refers to the cases when the phase velocity increases/decreases with the wave number. The dispersion relation for

the GO equation (1.1) is $\omega = ck - \beta k^3 + \gamma/k$, where ω is the frequency and k is the wave number of a linear wave of infinitesimal amplitude. From this dispersion relation it follows that the phase velocity is $V_{ph} \equiv \omega/k = c - \beta k^2 + \gamma/k^2$. The small-scale asymptotic ($\lambda \to 0, k \to \infty$) of this formula, $V_{ph} \approx -\beta k^2$, shows that the small-scale dispersion is positive when β is negative and vice versa.

4.1. Soliton solution to the GO equation with positive dispersion

The first example pertains to the soliton solution of the GO equation with positive small-scale dispersion ($\beta < 0$). Soliton solutions does not exist in the case of positive β at all provided that γ is positive (see, e.g., [5]), but in the case of $\beta < 0$ solitons can exist and can be constructed numerically using, for instance, the Petviashvili iterative method [13,18,20]. We describe first this method in application to the GO equation and then construct a soliton solution which will be used further as the initial condition for the non-stationary code.

4.1.1. The Petviashvili method for the numerical solution of the GO equation

For the stationary solutions of Eq. (1.1), i.e. solutions depending on one variable $\xi = x - Vt$, one can rewrite that equation in the following form:

$$\frac{d^2}{d\xi^2}\left[(c-V)\,u + \frac{\alpha}{2}u^2 + \frac{\alpha_1}{3}u^3 + \beta\frac{d^2u}{d\xi^2}\right] = \gamma u. \tag{4.1}$$

Let us make a transformation of variables to reduce this equation to the dimensionless form:

$$\zeta = \xi\sqrt{\frac{c-V}{\beta}}, \quad v = -\frac{\alpha u}{2\,(c-V)}. \tag{4.2}$$

After that Eq. (1.1) in new variables reads

$$\frac{d^2}{d\zeta^2}\left[v - v^2 + \delta v^3 + \frac{d^2v}{d\zeta^2}\right] = \sigma v, \tag{4.3}$$

where $\delta = 4\alpha_1\,(c-V)\,/\left(3\alpha^2\right)$ and $\sigma = \beta\gamma/\,(c-V)^2$.

Let us make a Fourier transformation of this equation on ζ:

$$\left(k^4 - k^2 - \sigma\right)\hat{F}(v) = -k^2\left[\hat{F}\left(v^2\right) - \delta\hat{F}\left(v^3\right)\right], \tag{4.4}$$

where

$$\hat{F}(v) = \frac{1}{\sqrt{2\pi}}\int\limits_{-\infty}^{+\infty} v(\zeta)e^{ik\zeta}\,d\zeta$$

stands for Fourier transformation of the function $v(\zeta)$.

Multiply now this equation by $\hat{F}(v)$ and integrate it over k from minus to plus infinity assuming that function $\hat{F}(v)$ is real (this corresponds to the assumption that function $v(\zeta)$ is even). Then we can define a functional

$$M\left[v(\zeta)\right] = -\frac{\int\limits_{-\infty}^{+\infty}\left(k^4 - k^2 - \sigma\right)\left[\hat{F}(v)\right]^2\,dk}{\int\limits_{-\infty}^{+\infty}k^2\left[\hat{F}\left(v^2\right) - \delta\hat{F}\left(v^3\right)\right]\hat{F}(v)\,dk}, \tag{4.5}$$

which represents a ratio of the left-hand side to right-hand side of the integrated Eq. (4.4). If $v(\zeta)$ is an exact solution of Eq. (4.3), then, obviously, $M = 1$. Thus, M can be treated as a measure of a closeness of a function $v(\zeta)$ to the exact solution.

In the spirit of the Petviashvili method [18] let us construct an iteration scheme presenting Eq. (4.4) in the form

$$\hat{F}(v)_{n+1} = -\frac{k^2}{k^4 - k^2 - \sigma}\left[\hat{F}\left(v_n^2\right) - \delta\hat{F}\left(v_n^3\right)\right] M^p\left[v_n\right]. \tag{4.6}$$

Here index $n = 0, 1, 2, \ldots$ stands for the iteration number; M^p with p being some real value plays a role of a stabilizing factor which provides a convergence of the iterative scheme (4.6) for any pulse-type start function $v_0(\zeta)$. Without this factor or, equivalently, with $p = 0$, the iterative scheme diverges and does not provide any solution. In relatively simple cases when there is only one power-type function v in the right-hand side of Eq. (4.6), e.g., $\hat{F}\left(v^q\right)$, where q is an arbitrary positive number, a strong mathematical criterion can be obtained for the exponent p of the stabilising factor which provides convergence of the iterative scheme, $1 < p < (q+1)/(q-1)$, and the fastest convergence occurs at $p = q/(q-1)$ [17] (e.g., for the equation with pure quadratic nonlinearity, $q = 2$, the fastest convergence occurs at $p = 2$, whereas for the equation with pure cubic nonlinearity, $q = 3$, the fastest convergence occurs at $p = 3/2$).

The convergence of iterations to any solution can be controlled with the help of the parameter $\mathcal{E} = |1 - M|$ characterising the discrepancy of the solution. If this parameter becomes less than some small quantity $\varepsilon \ll 1$, iterations can be terminated.

Note there are no zeros in the bi-quadratic polynomial in the denominator of Eq. (4.6) if its discriminant is negative, $D = 1 + 4\sigma < 0$ (in this case the polynomial is always positive). Hence the condition $\sigma < -1/4$ guaranties the absence of a singularity in Eq. (4.6).

4.1.2. Validation of the numerical codes

In our case with a complicated non-power nonlinearity (the sum of quadratic and cubic terms), the value of the parameter p can be taken between $p = 3/2$ and $p = 2$. In the following computations it was taken $p = 7/4$ and fairly fast convergence to the soliton solution was found. The Gaussian function $v_0(\zeta) = \exp\left(-\zeta^2/4\right)$ was used to start-up the iterative process. After 19 iterations with $\delta = 1/15$ and $\sigma = -0.4$ (this corresponds to the following set of coefficients in Eq. (4.1): $c = 0, \alpha = 1, \alpha_1 = -1, \beta = 1, \gamma = 10^{-3}$, and $V = 0.05$), the iterative process was terminated with the discrepancy $\mathcal{E} < 10^{-4}$. Note that with $\sigma = -0.4$, the discriminant of the bi-quadratic polynomial in the denominator of Eq. (4.6) $D = -0.6 < 0$, thus the absence of a singularity in that equation is guaranteed. The convergence process to the soliton solution is shown in Fig. 5 in terms of $\mathcal{E}_n$ versus the iteration number n, and the solution obtained is presented in Fig. 6 by solid red line.

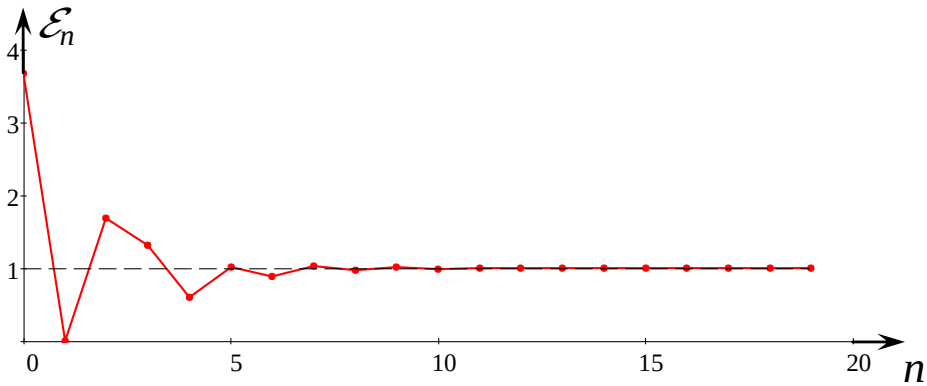

FIGURE 5. The solution discrepancy versus the iteration number for the soliton solution shown in Fig. 6 with the set of parameters indicated in the text.

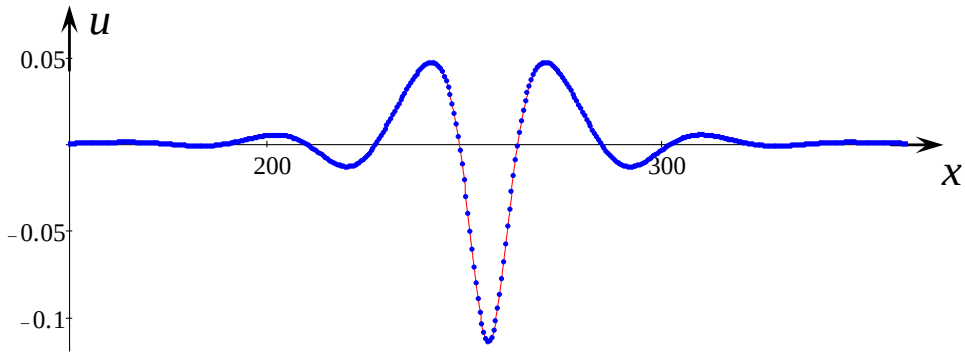

FIGURE 6. Soliton solution to the GO equation with positive small-scale dispersion ($\beta < 0$).

This solution was used then as the initial condition for Eq. (1.1) which was solved numerically with the periodic boundary conditions by the transient code developed on the basis of the numerical scheme (2.5). The spatial interval in both codes was $L = 512$, and the total number of grid points was $N = 2048$. The solution obtained in different instances of time was the same as at the initial moment with only the difference in its spatial position. The soliton moved along the axes x with the speed $V_{num} = 4.998 \cdot 10^{-2}$, which is very close to theoretically predicted value $V_{theor} = 0.05$. Blue dots in Fig. 6 show the soliton at $t = 10,250$ when it came back to the initial position after travelling one whole spatial period $L = 512$. As one can see, there are no visible differences between the initial function and the solution at $t = 10,250$.

Thus, one may conclude that on one hand the solution obtained with the transient numerical code confirms that the solution numerically obtained by the Petviashvili method is indeed stationary – nothing happening with it in the process of propagation. On the other hand, one may say that the transient numerical code works correctly and reproduces the stationary soliton solution independently obtained by the Petvishvili method. This solution stationary moves with the theoretically predicted velocity up to 0.04% accuracy.

In the process of numerical solution, the integral quantities I_1, I_2, and I_3 were tested and it was discovered that they remain constants with the following accuracy (for details see Table 1):

- I_1 keeps zero with the maximal deviation $|I_1| < 5.4 \cdot 10^{-7}$;
- I_2 keeps constant with the maximal relative error less than $2.5 \cdot 10^{-4}$;
- I_3 keeps constant with the maximal relative error less than $5.1 \cdot 10^{-4}$;
- the soliton maximum remained constant with the maximal relative error less than $2.5 \cdot 10^{-4}$;
- the soliton minimum remained constant with the maximal relative error less than $9.8 \cdot 10^{-4}$.

As follows from the stability analysis of Sect. 3, the maximum value of the most "dangerous" root λ_2 with the chosen set of parameters of Eq. (1.1) and $h = 0.25$, $\tau = 2.5 \cdot 10^{-4}$ is approximately 10^{-7}. This formally means that the scheme instability may come to the noticeable effect after about 10^6 time steps. The solution shown in Fig. 6 was obtained for $4 \cdot 10^7$ time steps, but there are still no any traces of the numerical instability. Apparently, this can be explained by the fact that the growth rate of the numerical instability is below the truncation error of computations, which is of the order of 10^{-6}. Hence, one can conclude that the scheme (2.5) is fairly robust under the appropriately chosen set of parameters.

Table 1. Dependence of integral characteristics on time for the soliton solution shown in Fig. 6.

Time	I_1	I_2	I_3	u_{max}	u_{min}	$x_{min}^{(*)}$
0	$2.1137 \cdot 10^{-15}$	0.264554	0.0156591	0.0466146	−0.114332	256
1,000	$5.00773 \cdot 10^{-7}$	0.264560	0.0156591	0.0466054	−0.114409	306
2,000	$4.50547 \cdot 10^{-7}$	0.264567	0.0156600	0.0466184	−0.114381	356
3,000	$4.61921 \cdot 10^{-7}$	0.264574	0.0156600	0.0466057	−0.114373	406
4,000	$5.33320 \cdot 10^{-7}$	0.264580	0.0156600	0.0466158	−0.114370	455.75
5,000	$5.23962 \cdot 10^{-7}$	0.264587	0.0156510	0.0466165	−0.114396	505.75
6,000	$4.66692 \cdot 10^{-7}$	0.264593	0.0156610	0.0466166	−0.114415	43.75
7,000	$4.24939 \cdot 10^{-7}$	0.264600	0.0156610	0.0466191	−0.114407	93.75
8,000	$4.78060 \cdot 10^{-7}$	0.264606	0.0156620	0.0466309	−0.114411	143.75
9,000	$4.25568 \cdot 10^{-7}$	0.264613	0.0156620	0.0466159	−0.114393	193.75
10,000	$4.74852 \cdot 10^{-7}$	0.264620	0.0156620	0.0466262	−0.114370	243.75

$^{(*)}$ The last column in this Table shows the position of the soliton center (minimum of function u) in the interval $0 \le x \le L = 512$.

4.2. Terminal decay of a KdV soliton due to influence of a large-scale dispersion

One more test on the scheme robustness can be undertaken with the help of approximate analytical solution to the Ostrovsky equation which describes a terminal decay of the KdV soliton due to influence of a large-scale dispersion proportional to γ. The Ostrovsky equation originally derived for the description of weakly nonlinear waves in a rotating ocean [14] can be treated as the particular case of the GO equation when the cubic nonlinear term in Eq. (1.1) is omitted ($\alpha_1 = 0$). As has been aforementioned, in the case of negative small-scale dispersion (this corresponds to the case of $\beta > 0$ in Eq. (2.1)), the Ostrovsky equation does not possess a pulse-type stationary solution [5,12]. However, if the large-scale dispersion is relatively small ($\gamma \ll 1$ in Eq. (1.1)), then one can consider smooth adiabatic evolution of the initial KdV soliton which leads to the terminal decay of the soliton in a finite time. This process has been studied

in [8, 9]. However, later it was shown that when the initial soliton decays, it produces non-stationary wave train, which after long-term evolution eventually evolves into the envelope soliton described by the nonlinear Shrödinger equation [10]. Below we briefly reproduce the approximate solution [8,9] describing only the initial stage of soliton evolution which ends up by its terminal decay. The same process will be modelled then numerically with the help of a Fortran code based on the numerical scheme described above in Sect. 3. Results obtained will be compared against the approximate analytical solution.

4.2.1. Approximate soliton solution of the Ostrovsky equation

Consider now Eq. (2.1) assuming that the coefficient γ is very small in comparison to all other coefficients. When $\gamma = 0$, this equations reduces to the usual KdV equation, one of stationary solutions of which is a soliton sitting on the arbitrary constant pedestal d [1, 22]:

$$u = \frac{A}{\cosh^2 (x - Vt)/\Delta} + d, \tag{4.7}$$

where the characteristic soliton width

$$\Delta = \sqrt{\frac{12\beta}{\alpha A}} \quad \text{and speed} \quad V = \alpha(d + A/3)$$

are related to the soliton amplitude A.

If $\gamma \neq 0$, but sufficiently small, $\gamma \ll 1$, then the soliton solution (4.7) is no longer valid, strictly speaking. However, if the KdV soliton is structurally stable (and this is the matter of fact), then it cannot be destroyed immediately under small perturbation. In this case one can expect rather gradual adiabatic variation of the soliton with time when it preserves its shape and relationships between the parameters (amplitude, velocity, and width) at any instant of time. The pedestal d should be adjusted to the soliton amplitude to satisfy the zero mean-value condition, $I_1 = 0$ (see above). This leads to $d = -A\,(2\Delta/L)\tanh\,(L/2\Delta)$, where L is the length of the spatial interval. For the infinite interval the pedestal is obviously zero, and it is very small if $L \gg \Delta$. Considering further namely this case of very large, but finite spatial interval, we can put $d \approx 0$ in the analytical calculations (but not in the numerical simulations!).

To calculate time variation of soliton parameters one needs to apply the well known asymptotic perturbation approach described, in particular, in Ref. [8]. This approach actually reduces to the energy balance equation which can be readily derived from Eq. (2.1). To derive it, let us multiply Eq. (2.1) by u and integrate then the resultant equation over x in the infinite limits. Taking into account that we consider soliton solution vanishing at the infinity, we obtain (all other terms vanish after the integration):

$$\frac{1}{2}\frac{d}{dt}\int\limits_{-\infty}^{+\infty} u^2\,dx = \gamma \int\limits_{-\infty}^{+\infty}\left[u\left(\int\limits_{-\infty}^{x} u\,dx' + C\right)\right]dx. \tag{4.8}$$

Substitute now into this equation soliton solution (4.7) with $d = 0$ assuming that its amplitude is a slowly varying function of time. The integral in the left-hand side of this equation can be readily calculated:

$$\frac{1}{2}\frac{d}{dt}\int\limits_{-\infty}^{+\infty} u^2\,dx = \frac{d}{dt}\left(A^2\Delta\int\limits_{0}^{+\infty}\frac{d\xi}{\cosh^4\xi}\right) = \frac{2}{3}\sqrt{\frac{12\beta}{\alpha}}\frac{dA^{3/2}}{dt} = \sqrt{\frac{12\beta A}{\alpha}}\frac{dA}{dt}. \tag{4.9}$$

The integrals in the right-hand side of Eq. (4.8)can be calculated step-by-step. Consider first the inner integral; by substitution the soliton solution (4.7) into it we obtain:

$$\int\limits_{-\infty}^{x} u\,dx' + C = A\Delta\int\limits_{-\infty}^{x}\frac{d\xi}{\cosh^2\xi'} + C = A\Delta\left(\tanh\frac{x}{\Delta} + 1\right) + C. \tag{4.10}$$

The constant C must be chosen such that the perturbation is absent far away in front of the soliton. When a soliton propagates under the influence of a small perturbative term proportional to γ within the framework of Eq. (2.1), it generates trailing waves. The dispersion relation for such waves follows from the linearised version of Eq. (2.1): $\omega = \gamma/k - \beta k^3$, where ω is the wave frequency and k is the wavenumber. Then the group velocity is $V_g \equiv d\omega/dk = -\gamma/k^2 - 3\beta k^2$. As one can see, the group velocity is negative for all k if β and γ are both positive (we consider below namely this case of negative small-scale dispersion). In such case small perturbations which are generated by the soliton in the course of its propagation run to the left and there are no any perturbations in front of the soliton. Hence, we have to put $C = -2A\Delta$ and Eq. (4.10) becomes

$$\int\limits_{-\infty}^{x} u\,dx' + C = A\Delta \int\limits_{-\infty}^{x} \frac{d\xi}{\cosh^2 \xi'} + C = A\Delta \left(\tanh \frac{x}{\Delta} - 1\right). \tag{4.11}$$

Now we have to calculate the outer integral in Eq. (4.8) using the result obtained in Eq. (4.11):

$$\gamma A^2 \Delta^2 \int\limits_{-\infty}^{+\infty} \frac{\tanh \xi - 1}{\cosh^2 \xi}\, d\xi = -2\gamma \frac{12\beta A}{\alpha} \int\limits_{0}^{+\infty} \frac{d\xi}{\cosh^2 \xi} = -24 \frac{\beta\gamma}{\alpha} A. \tag{4.12}$$

Ultimately, Eq. (4.8) reads

$$\frac{dA}{dt} = -2\gamma \sqrt{\frac{12\beta A}{\alpha}} \tag{4.13}$$

and its solution is

$$A = A_0 \left(1 - t/T_{ext}\right)^2, \tag{4.14}$$

where $T_{ext} = (1/\gamma)\sqrt{\alpha A_0/(12\beta)} = 1/(\gamma \Delta_0)$ is the soliton extinction time, and Δ_0 is the soliton width at the initial instant of time.

Due to terminal decay of a soliton, one can calculate the total traversed path using the relationship between soliton amplitude and velocity, $V(t) = \alpha A(t)/3$ (see the formula after Eq. (4.7) with $d = 0$) given the framework of the adiabatic theory:

$$L_{ext} = \int\limits_{0}^{T_{ext}} V(t)\,dt = \frac{\alpha}{3} \int\limits_{0}^{T_{ext}} A(t)\,dt = \frac{\alpha A_0}{3} \int\limits_{0}^{T_{ext}} \left(1 - \frac{t}{T_{ext}}\right)^2 dt = \frac{(\alpha A_0)^{3/2}}{18\gamma\sqrt{3\beta}}. \tag{4.15}$$

However, as has been mentioned above, it was shown that in the process of terminal decay the soliton produces non-stationary wave train, which after long-term evolution eventually evolves into the envelope soliton described by the nonlinear Shrödinger equation [10]. This transformation is beyond the scope of this paper.

4.2.2. Numerical results and their comparison against the analytical solution

To study the process of soliton evolution numerically within the Ostrovsky equation (2.1) with $\alpha_1 = 0$, we have to satisfy the zero mean-value constraint: $I_1 = 0$ (see above). To this end we consider soliton solution (4.7) on a pedestal d, which is chosen such that the condition $\langle u(t,0)\rangle = 0$ is fulfilled at the initial instant of time. This gives $d = -A_0\,(2\Delta_0/L)\tanh\,(L/2\Delta) \approx 2A_0\,(\Delta_0/L)$, where the approximate equality is actually very precise as we consider a solution on a spatial interval $L \gg \Delta_0$ so that $\tanh(L/2\Delta_0) \approx 1$ with a high accuracy. The value of the pedestal is negligibly small (but of the principle importance for the numerical calculations) if L is very large.

A numerical calculation with the initial condition of a soliton (4.7) sitting on the properly adjusted pedestal was undertaken with the periodic boundary conditions. The following set of parameters has

been chosen: $\alpha = \beta = 1$, $\alpha_1 = 0$, $\gamma = 10^{-4}$, $L = 5 \cdot 10^3$, $h = 0.5$, $\tau = 4 \cdot 10^{-3}$ (thus, the dimensionless parameters controlling the stability of the numerical scheme are $B = \beta\tau/h^3 = 0.032$ and $\Gamma = \gamma h^4/4\beta = 1.56 \cdot 10^{-6}$). Initial soliton amplitude was $A_0 = 1$, which results in $\Delta_0 = 2\sqrt{3}$, $V_0 = 1/3$, and the pedestal $d = -8\sqrt{3} \cdot 10^{-4} \approx -1.39 \cdot 10^{-3}$. Figure 7 illustrates soliton evolution at different times. One can clearly see that the leading pulse gradually decreases keeping the shape of a KdV soliton. A very intense trailing wave train is generated behind the leading pulse in the process of soliton propagation, whereas there are no perturbations in front of the leading pulse within the considered time interval (such perturbations, however, appear later due to periodic boundary conditions).

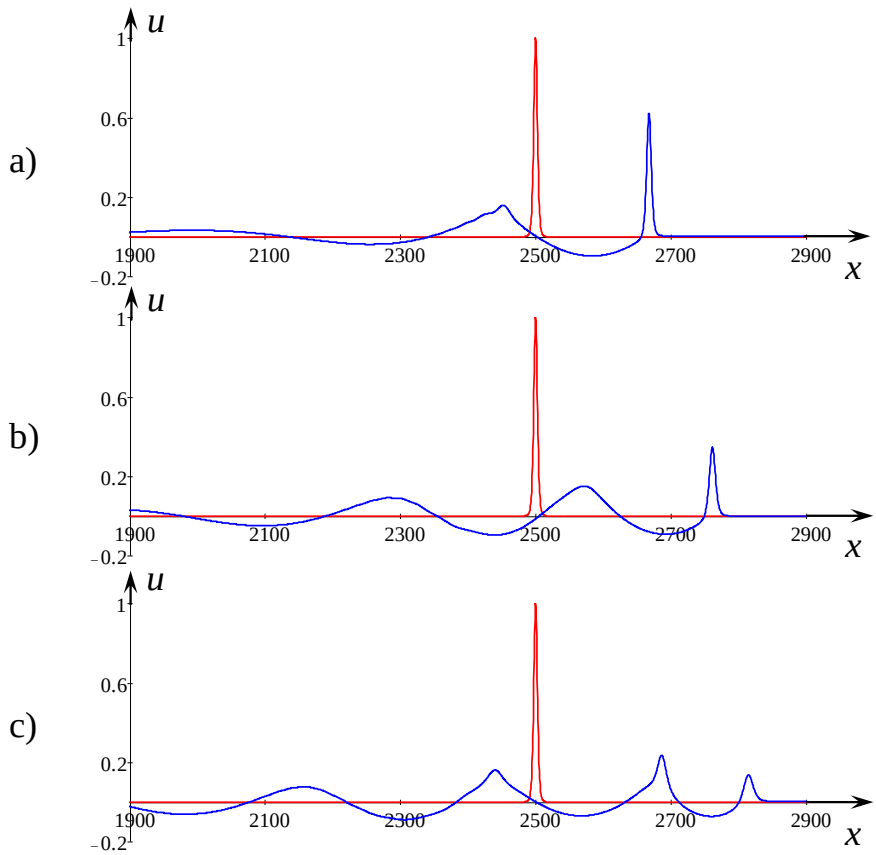

FIGURE 7. Fragments of numerical solutions of Eq. (2.1) at different instants of time (the total spatial interval $L = 5,000$). Red lines in each frame represent the initial KdV soliton (4.7) on a pedestal (the pedestal is so small, $d \approx -1.39 \cdot 10^{-3}$ that it is practically invisible in this scale). Blue lines represent numerical solutions at: $t = 630$ (frame a); 1230 (frame b); and 1950 (frame c).

Numerically obtained dependence of the leading pulse amplitude on time is shown in Fig. 8 (red dots); the analytical solution (4.14) is also shown in that figure by solid line 1. The theoretical prediction for the soliton extinction time is $T_{ext} = (\gamma\Delta_0)^{-1} \approx 2.89 \cdot 10^3$. As one can see, the numerical data agree very well with the analytical solution (4.14) up to $\gamma t \approx 0.18$. The agreement becomes worse at larger t when the leading pulse becomes very small. This can be explained by the influence of trailing large-scale waves which appear in front of the leading pulse due to periodic boundary conditions.

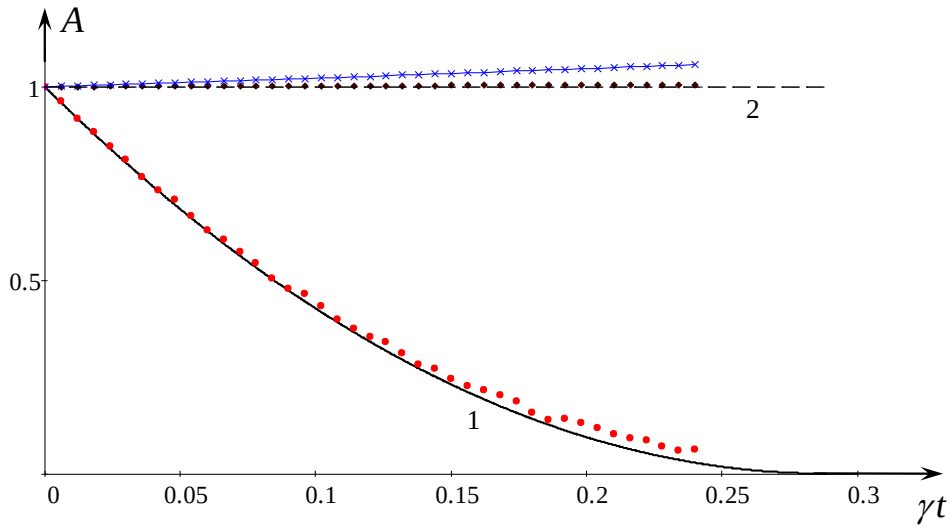

FIGURE 8. Dependence of the soliton amplitude on normalised time as per Eq. (4.14) (solid line 1). Red dots are numerical data for the amplitude of the leading pulse, small black diamonds represent data for the normalised integral $I_2(t)/I_2(0)$, and crosses – the data for the normalised integral $I_3(t)/I_3(0)$. Dashed line 2 is just a constant value reference line for the comparison of the relative integral quantities with the unity.

A position of the leading-pulse maximum versus time has been recorded in the course of computations. The results obtained are shown in Fig. 9. As follows from this figure, the pulse moves non-uniformly, gradually decelerating with time. Its velocity can be roughly estimated at the recorded instances of time using finite differences: $V_p \approx \Delta x/\Delta t$. As the pulse amplitude has been also recorded at the corresponding instances of time, we have obtained a dependence of pulse velocity on amplitude. This dependence is shown in Fig. 10, where similar dependence for the KdV soliton, $V = \alpha A/3$, is also shown by the solid line.

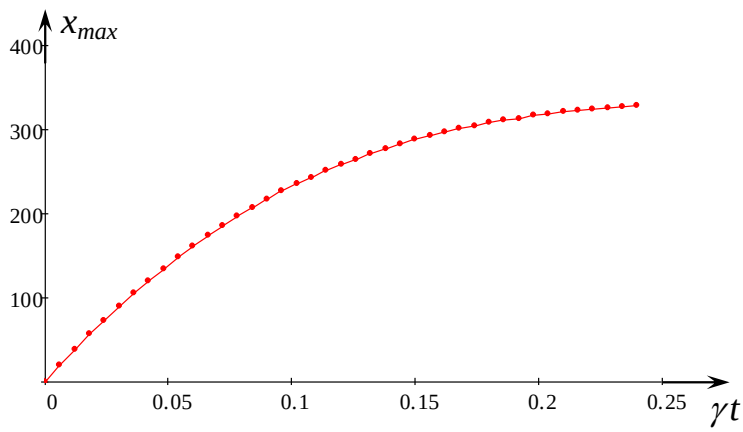

FIGURE 9. Dependence of the leading pulse position on normalised time.

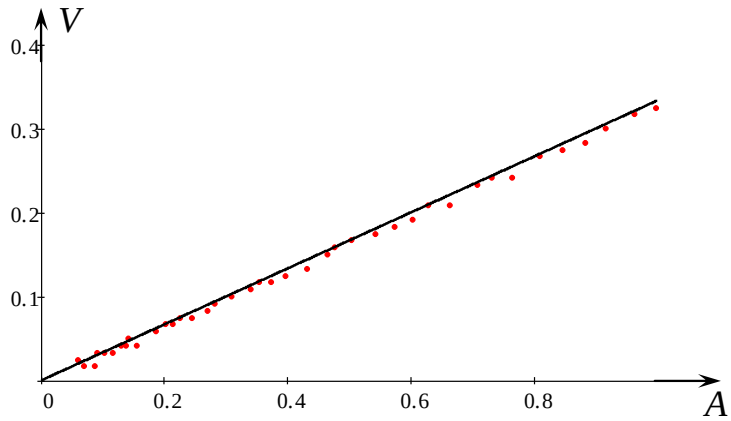

FIGURE 10. Theoretical dependence of soliton speed on the amplitude (solid line) and results of computations for the leading pulse.

As one can see, there is a good agreement between the theoretical dependence for the KdV soliton and numerical data for the leading pulse. This underpins the assumption that in the process of decay, the leading pulse keeps the shape of a KdV soliton experiencing just an adiabatic change and keeping the characteristic relationship between main soliton parameters – amplitude, width and velocity (see formulae after Eq. (4.7)).

In the course of numerical solution, the integral quantities I_1, I_2, and I_3 were tested again and it was discovered that they remain constant with the following accuracy (for details see Table 2):

- I_1 keeps zero with the maximal deviation $|I_1| < 1.19 \cdot 10^{-12}$;
- I_2 keeps constant with the maximal relative error less than $3.85 \cdot 10^{-3}$;
- I_3 keeps constant with the maximal relative error less than $2.6 \cdot 10^{-2}$.

Dependences of normalised integral quantities $I_2(t)/I_2(0)$ and $I_3(t)/I_3(0)$ from Table 2 (and even with the more frequent time step) are shown in Fig. 8. It is seen that the used numerical scheme preserves the quantity I_2 quite well, whereas the Hamiltonian, $I_3(t)$, gradually growths with time.

As follows from the stability analysis of Sect. 3, the maximum value of the most "dangerous" root λ_2 with the chosen set of parameters of Eq. (1.1) and $h = 0.5$, $\tau = 4 \cdot 10^{-3}$ is approximately $5 \cdot 10^{-7}$. This formally means that the scheme instability may come to the noticeable effect after about 10^5 time steps. The solution shown in Fig. 7 was obtained for $6 \cdot 10^5$ time steps and looks quite stable despite of relatively poor conservation of the Hamiltonian I_3 (see crosses in Fig. 8). It is not surprising as the Hamiltonian contains a derivative of u, and its finite-difference approximation causes a numerical error which is much higher than the error of numerical calculation of the function u itself.

Thus, this test also evidencing that the numerical scheme (2.5) is fairly robust when the parameters are chosen appropriately.

5. Conclusion

A simple explicit numerical scheme is proposed for the solution of the Gardner-Ostrovsky equation. The proposed numerical scheme generalises the well-known finite-difference scheme [3], which has been successfully used for the solution of the KdV equation. The scheme is of the second order accuracy both on temporal and spatial variables. The stability analysis of the scheme is presented for infinitesimal perturbations. It has been shown that the scheme is formally unstable, for the long-term calculations. However, within the limited time interval computations may be accurate as the development of the

numerical instability may be very weak due to small value of its growth rate. Moreover, if the growth rate is below the accuracy of numbers truncation, then the instability unlikely can manifest itself. The derived formula allows one to estimate the growth rate numerically. Examples of calculations with the periodic boundary conditions have been presented. They confirm the robustness of the scheme.

Table 2. Dependence of integral characteristics on time for the numerical solution shown in Fig. 7 (the data in the Table are shown only for each forth recorded time interval).

Time	I_1	I_2	I_3	u_{max}
0	$-1.18664 \cdot 10^{-12}$	4.6092	2.91508	0.998614
240	$5.68989 \cdot 10^{-16}$	4.61422	2.92953	0.845437
480	$2.27995 \cdot 10^{-14}$	4.61798	2.94492	0.708042
720	$-2.74173 \cdot 10^{-14}$	4.62068	2.96103	0.573522
960	$-2.24300 \cdot 10^{-14}$	4.62265	2.97764	0.464514
1,200	$-1.27598 \cdot 10^{-13}$	4.62408	2.99461	0.354007
1,440	$-2.20303 \cdot 10^{-14}$	4.62514	3.01188	0.270220
1,680	$-5.28137 \cdot 10^{-14}$	4.62595	3.02939	0.201786
1,920	$-3.69323 \cdot 10^{-14}$	4.62657	3.04713	0.141434
2.160	$6.10085 \cdot 10^{-14}$	4.62690	3.06511	0.090748
2,400	$9.14147 \cdot 10^{-14}$	4.62693	3.08336	0.063079

Acknowledgements. This paper was partially implemented within the framework of the visitorship program provided by the MPIPKS (Dresden, Germany) for one of the authors (Y. S.) in June 2010. Y. S. is grateful to the MPIPKS for the hospitality and possibility to work at the Institute in the indicated period. The authors are also indebted to Prof. Ramon Fernandez-Feria from the E.T.S. Ingeniería Industrial (University of Malaga, Spain) for the critical reading of the paper and useful comments.

References

[1] M.J. Ablowitz, H. Segur. Solitons and the Inverse Scattering Transform. SIAM, Philadelphia, 1981.

[2] J. Apel, L.A. Ostrovsky, Y.A. Stepanyants, J.F. Lynch. *Internal solitons in the ocean and their effect on underwater sound*, J. Acoust. Soc. Am., 121 (2007), No. 2, 695–722.

[3] Yu. Berezin. Modelling Nonlinear Wave Processes. VNU Science Press, 1987.

[4] M. Dehghan, F. Fakhar-Izadi. *The spectral collocation method with three different bases for solving a nonlinear partial differential equation arising in modeling of nonlinear waves*, Math. Comp. Modelling, 53 (2011), 1865–1877.

[5] V.M. Galkin, Yu.A. Stepanyants. *On the existence of stationary solitary waves in a rotating fluid*, J. Appl. Maths. Mechs., 55 (1991), No 6, 939–943 (English translation of the Russian journal "Prikladnaya Matematika i Mekhanika").

[6] O.A. Gilman, R. Grimshaw, Yu.A. Stepanyants. *Approximate analytical and numerical solutions of the stationary Ostrovsky equation*, Stud. Appl. Math., 95 (1995), No 1, 115–126.

[7] O.A. Gilman, R. Grimshaw, Yu.A. Stepanyants. *Dynamics of internal solitary waves in a rotating fluid*, Dynamics. Atmos. and Oceans, 23 (1996), No 1–4, 403–411.

[8] R. Grimshaw, J.-M. He, L.A. Ostrovsky. *Terminal damping of a solitary wave due to radiation in rotational systems*, Stud. Appl. Math., 101 (1998), 197–210.

[9] R. Grimshaw, L.A. Ostrovsky, V.I. Shrira, Yu.A. Stepanyants. *Long nonlinear surface and internal gravity waves in a rotating ocean*, Surveys in Geophys., 19 (1998), 289–338.

[10] R. Grimshaw, K. Helfrich. *Long-time solutions of the Ostrovsky equation*, Stud. Appl. Math., 121 (2008), No 1, 71–88.

[11] P. Holloway, E. Pelinovsky, T. Talipova. *A generalised Korteweg-de Vries model of internal tide transformation in the coastal zone*, J. Geophys. Res. 104 (1999), No 18, 333–350.

[12] A.I. Leonov. *The effect of the Earth's rotation on the propagation of weak nonlinear surface and internal long oceanic waves*, Ann. New York Acad. Sci., 373 (1981), 150–159.

[13] M.A. Obregon, Yu.A. Stepanyants. *Oblique magneto-acoustic solitons in rotating plasma*, Phys. Lett. A, 249, (1998), No 4, 315–323.

[14] L.A. Ostrovsky. *Nonlinear internal waves in a rotating ocean*, Oceanology, 18 (1978), 119–125. (English translation of the Russian journal "Okeanologiya").

[15] L.A. Ostrovsky, Yu.A. Stepanyants. *Nonlinear surface and internal waves in rotating fluids*. In: "Nonlinear Waves 3", Proc. 1989 Gorky School on Nonlinear Waves, (1990), 106–128. Eds. A.V. Gaponov-Grekhov, M.I. Rabinovich and J. Engelbrecht, Springer-Verlag, Berlin–Heidelberg.

[16] L.A. Ostrovsky, Yu.A. Stepanyants. *Internal solitons in laboratory experiments: Comparison with theoretical models*, Chaos, 15, (2005) 037111, 28 p.

[17] D.E. Pelinovsky, Yu.A. Stepanyants. *Convergence of Petviashvili's iteration method for numerical approximation of stationary solutions of nonlinear wave equations*, SIAM J. Numerical Analysis, 42, (2004), 1110–1127.

[18] V.I. Petviashvili, O.V. Pokhotelov. Solitary Waves in Plasmas and in the Atmosphere. Gordon and Breach, Philadelphia, 1992.

[19] Yu.A. Stepanyants. *On stationary solutions of the reduced Ostrovsky equation: Periodic waves, compactons and compound solitons*, Chaos, Solitons and Fractals, 28, (2006), 193–204.

[20] Yu.A. Stepanyants, I.K. Ten, H. Tomita. *Lump solutions of 2D generalised Gardner equation*. In: "Nonlinear Science and Complexity", Proc. of the Conference, Beijing, China, 7–12 August 2006, 264–271. Eds. A.C.J. Luo, L. Dai and H.R. Hamidzadeh, World Scientific, 2006.

[21] V.O. Vakhnenko. *High-frequency soliton-like waves in a relaxing medium*, J. Math. Phys., 40, (1999), 2011–2020.

[22] G.B. Whitham. Linear and Nonlinear Waves. John Wiley & Sons, 1974.

[23] T. Yaguchi, T. Matsuo, M. Sugihara. *Conservative numerical schemes for the Ostrovsky equation*, J. Comp. Appl. Maths., 234, (2010), 1036–1048.